Expanded solid matter: Two-dimensional LJ modeling

F.H. Stillinger *, D.K. Stillinger

Department of Chemistry, Princeton University, Princeton, NJ 08544, USA

Abstract

The existence and technological importance of expanded solid forms of matter such as aerogels indicate the need for related theoretical and simulational modeling. As an elementary step in this direction, we have examined a concurrent (as opposed to sequential) aggregation process for Lennard-Jones particles in two dimensions, starting from dilute initial conditions. Steepest-descent mapping on the multi-particle potential energy surface to mechanically stable minima ("inherent structures") is the basic tool involved. The results obtained for $N = 400$ particles display a wide diversity of extended, branched, and void-enclosing patterns that typically include frozen-in strains. Not surprisingly, the energies of these inherent structures tend to lie toward the high end of the full range of available inherent structure energies for 400 Lennard-Jones particles. Furthermore, the geometric characteristics observed for these low-density aggregates support theoretical arguments indicating that the number of distinct inherent structures in free space rises faster than exponentially with particle number N.
© 2005 Elsevier Ltd. All rights reserved.

Keywords: Aerogels; Lennard-Jones model; Inherent structures; Fractal clusters; Burgers vector; Minimization routines

1. Introduction

As a result of specialized formation circumstances, a wide variety of normally dense solid materials can be rendered into highly expanded, but still solid forms. Geometrically this involves spatial inhomogeneity by virtue of incorporated regions of empty space, with length scales ranging from nanometers upward into the macroscopic regime. Perhaps the most spectacular example of expanded solid matter is provided by the family of silica-based aerogels ("solid smoke") that can have mass densities less than 1% of conventional fused silica (Frick, 1988; Pekala and Hrubesh, 1995). Other examples include solidified polymer foams such as styrofoam (Brydson, 1989), spongy metals created by radiation damage (Sheely, 1967; Engh, 1992), and carbon allotropes containing "buckyballs" (Krätschmer et al., 1990) or single-walled nanotubes (Kong et al., 1998). Mesoporous solids can also be formed by low-temperature deposition of simple materials such as nitrogen and krypton on suitable substrates (Kiryukhin et al., 1997). The existence of these expanded solid materials obviously raises a group of intriguing scientific and technical questions, such as those concerning the distribution of local geometries within their interiors, the sensitivity of local structure to formation conditions, the mechanical

---

* Corresponding author.
  E-mail address: fhs@princeton.edu (F.H. Stillinger).

and thermodynamic properties of the expanded solids, and how those expanded solids interact with various forms of radiation and with invading fluids. And coupled to each of these questions is how their answers depend upon details of the specific interaction potentials that operate among the particles constituting the materials of interest.

While far from attempting to address all of these questions, the present paper presents a simple modeling approach that reveals some aspects of the complexity at the atomic/molecular length scale that expanded solid materials can exhibit. In the interests of conceptual simplicity and ease of visualization, the results reported below are restricted to two spatial dimensions. However, complex many-particle cooperative effects arise even in this simple circumstance, and manage to create a rich panoply of geometric patterns. As will become apparent to the reader, the approach described below is amenable to extension in several significant directions, and eventually deserves some attention beyond what we are able to describe here.

Section 2 outlines features of the Lennard-Jones interaction model that are relevant to our calculations. Section 3 describes the formation process employed to create mechanically stable expanded structures. This process is a configurational mapping operation, using a multi-dimensional steepest-descent procedure that has had beneficial applications previously in various condensed-phase theoretical and simulational studies. Section 4 specifies the technical details involved in setting up and carrying out the numerical aspects of this project, while Section 5 presents and analyzes results. A final Section 6 discusses several issues raised by those results, and offers suggestions for the most useful directions for future study in this area.

2. LJ model

We consider a collection of N structureless particles confined to a plane of infinite extent in all directions. The N particles interact with one another according to a potential energy function Φ that comprises a sum of particle-pair contributions:

$$\Phi(\mathbf{r}_1 \ldots \mathbf{r}_N) = \sum_{i<j} v(r_{ij}). \qquad (2.1)$$

Here $\mathbf{r}_i$ denotes the position of particle i in the infinite plane, and r_{ij} is the scalar distance between particles i and j. The pair interaction function will be assigned the Lennard-Jones (LJ) form (Jones, 1924):

$$v(r) = 4\varepsilon[(\sigma/r)^{12} - (\sigma/r)^6]. \qquad (2.2)$$

This choice involves repulsion at very short distance, but attraction at intermediate distance that rapidly dies away with increasing pair separation, though remaining non-vanishing at all finite distances. The energy (ε) and distance (σ) units in v have been set equal to unity for the purposes of this study, and as a result v has a unit-depth minimum at pair separation

$$r_{\min} = 2^{1/6} \cong 1.12246. \qquad (2.3)$$

When a large number N of these LJ particles have the opportunity to seek and adopt the most favorable (i.e. lowest Φ) arrangement in the plane, they produce the compact triangular lattice, with each particle surrounded by six nearest neighbors. This periodic structure with vanishing pressure represents a compromise between the repulsive cores of the particles which by themselves force those particles apart, and the attractive forces that draw them as closely together as possible. A straightforward calculation for the triangular lattice shows that the final result of this compromise Φ minimization produces a nearest-neighbor separation r_{nn} somewhat less than $r_{\min}$ shown above:

$$r_{nn} \cong 1.11142 \qquad (2.4)$$

and at this nearest-neighbor separation the triangular lattice has the following value of the interaction potential per particle:

$$\lim_{N \to \infty} \Phi/N = -3.38342. \qquad (2.5)$$

All other spatial arrangements of the LJ particles exhibit higher values of Φ/N.

Because the collection of N particles resides in the infinite plane, Φ possesses several elementary invariances owing to symmetry. Clearly it is unchanged by translation of all particle positions $\mathbf{r}_1 \ldots \mathbf{r}_N$ by a common arbitrary vector displacement. It is also unchanged by arbitrary rotation of the set of positions. Inversion or mirror-imaging of the particle configuration also leaves Φ unchanged. Finally, Φ is invariant to all $N!$ permutations of the identical particles.

3. Mapping to potential minima

Present interest concerns mechanically stable arrangements of N particles in the plane, where the interactions have the LJ form specified by Eqs. (2.1) and (2.2). These arrangements are all local

minima of the full N-body potential Φ, and have no net force on any particle. All of the minima can in principle be accessed in the $2N$-dimensional configuration space of particle coordinates by a steepest descent trajectory on the "rugged Φ landscape", starting from some suitable particle arrangement, until the multi-dimensional gradient of Φ vanishes. The set of all starting configurations that map to the same minimum constitutes a "basin of attraction" for that minimum under the steepest descent process. The collection of all basins exhaustively covers the entire configuration space. Following the tradition established by frequent use of this procedure in various condensed matter physics and chemistry applications, the Φ minima will be called "inherent structures" (Giovambattista et al., 2002; Della Valle et al., 2003; Sheng and Ma, 2004).

Steepest descent trajectories can be parameterized by means of a virtual "time" parameter $0 \leqslant s < \infty$, where $s = 0$ corresponds to the initial configuration, and $s \to +\infty$ represents convergence to the relevant inherent structure. The set of particle positions $\mathbf{r}_1(s) \ldots \mathbf{r}_N(s)$ during this mapping operation obey the following set of coupled differential equations:

$$\mathrm{d}\mathbf{r}_i(s)/\mathrm{d}t = -\nabla_i \Phi[\mathbf{r}_1(s) \ldots \mathbf{r}_N(s)] \quad (1 \leqslant i \leqslant N).$$
$$(3.1)$$

Here the differential operator ∇_i denotes the gradient with respect to the coordinates of particle i. This set of Eq. (3.1) simply states that particles displace by rates proportional to the respective forces that they experience, until all forces simultaneously vanish.

Enumerating all inherent structures, either analytically or numerically, for any given potential function largely remains an open problem, except for rather small N. However some general results are available. If the N particles are confined to a finite region so that the overall number density is $\rho > 0$, then as $N \to \infty$ at fixed ρ, the number Ω of distinct inherent structures (i.e. not counting particle permutations) rises essentially exponentially with N (Stillinger and Weber, 1983):

$$\ln \Omega(N, \rho) \sim \alpha(\rho)N \quad (\rho > 0, \ \alpha > 0). \tag{3.2}$$

Beside its indicated density dependence, the positive quantity $\alpha(\rho)$ depends as well on the specific interaction function involved.

The present study in principle concerns a finite number N of particles in the infinite plane, so the number density $\rho = 0$. Several arguments are available to indicate that $\alpha(\rho)$ diverges to infinity as $\rho \to 0$, implying that the extra space available for placing particles in mechanically stable arrangements permits the existence of a very large number of spatially extended inherent structures. Those arguments (Stillinger, 2001) indicate that asymptotic estimate (3.2) above needs to be replaced by the alternative form:

$$\ln \Omega(N, \rho = 0) \sim \gamma N \ln N \quad (\gamma > 0). \tag{3.3}$$

One of the objectives of the present study has been to verify the assumed existence of a large and diverse class of extended inherent structures for substantial collections of LJ particles. In this connection it is worth noting that the spatially most extended inherent structure for N particles with LJ interactions, and probably the inherent structure with the highest value of Φ/N, consists of a straight double row of particles. Fig. 1 illustrates this "needle" pattern. Numerical analysis readily verifies that indeed this arrangement is mechanically stable. Except near the ends where some dilation occurs, the near-neighbor distances are found to be 1.11452 (in the direction parallel to the needle axis) and 1.12011 (diagonally across the needle), both somewhat larger than the compact triangular crystal r_{nn} in Eq. (2.4) above. In the infinitely long needle limit, the binding energy per particle has the value:

$$\lim_{N \to \infty} [\Phi/N]_{\mathrm{needle}} = -2.11628. \tag{3.4}$$

The three-dimensional analog of this needle arrangement for LJ particles involves a stack of triangles whose planes are perpendicular to the needle axis, and which have a 60° twist from one layer to the next (Stillinger and Stillinger, 1990).
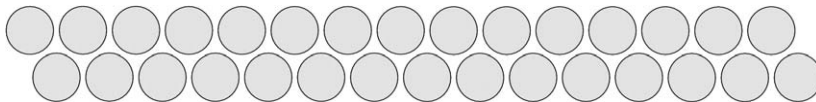

Fig. 1. Representative example of a mechanically stable needle cluster, in this case containing 30 LJ particles.

4. Numerical simulation

In order to investigate the kinds of inherent structures that the LJ model is capable of producing under low density conditions, we have applied a numerical implementation of the steepest descent mapping to a random initial configuration of $N = 400$ particles (following preliminary feasibility investigations with both $N = 100$ and 400). These particles were initially placed at random within the interior of a circle with radius 52.504 (in reduced units). The corresponding formal reduced density for this starting point is $\rho = 0.046188$, less than one-twentieth of the zero-temperature, zero-pressure value for the triangular crystal, $\rho_{\mathrm{tri}} = 0.93479$. Fig. 2 presents an example of such a starting configuration. Subsequently, all N particles in principle are free to move throughout the entire infinite plane.

Steepest descent trajectories, moving all 400 particles simultaneously toward an inherent structure, were generated by numerically approximating solutions to the basic equation set (3.1). This requires a lengthy sequence of direct incremental displacements for each particle by an amount proportional to the net force experienced by that particle:

$$\Delta \mathbf{r}_i(s + \delta s) \cong -\delta s \nabla_i \Phi[\mathbf{r}_1(s) \dots \mathbf{r}_N(s)]. \qquad (4.1)$$

At the beginning of a simulation of the type just described, it is almost always the case that at least one pair of the LJ particles has been randomly placed at very small separation, so that the members of such a pair exert very strong repulsive forces on one another. This is so even though the overall number density is small. Consequently, the earliest stage of numerical integration requires use of very small δs. After these close pairs move apart during this early stage (while other particles are virtually stationary), it then becomes possible to increase δs monotonically. However, experience has shown that an effective upper limit $\delta s = 4 \times 10^{-3}$ must be observed. Any substantial increase above this value leads to numerical instability, causing an explosive destruction of the clustering aggregate of particles.

Some insight into the operation of the steepest descent process emerges by considering its simplest application, namely the relative motion of a pair of LJ particles isolated from the remaining 398, and initially far enough from one another that only the attractive r^{-6} portion of their interaction is relevant. In this circumstance, their pair separation r
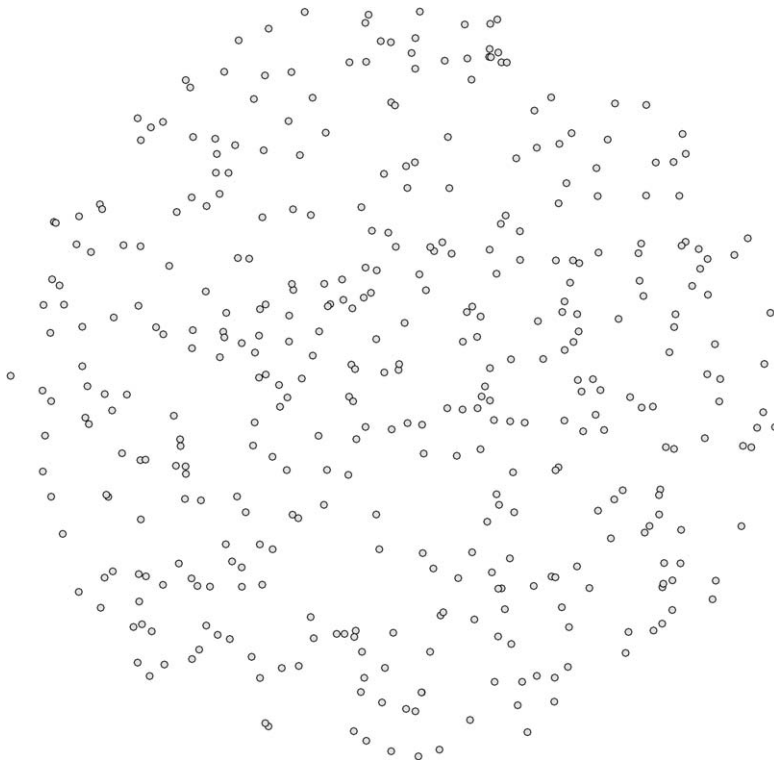

Fig. 2. Typical random starting configuration of 400 LJ particles confined to the interior of a circle with radius 52.504.

as a function of virtual time s will be described by the following differential equation:

$$dr(s)/ds = -48r^{-7}(s) \quad (4.2)$$

with solution:

$$r(s) = [r^8(0) - 384s]^{1/8}. \quad (4.3)$$

This result predicts that the amount of time s_1 that would have to elapse for pair distance r to decline to unity (when the repulsive part of the pair potential has become important) is:

$$s_1 \cong 2.1r^8(0). \quad (4.4)$$

If $r(0)$ is large, most of the elapsed time for the pair is spent with extremely slow drift toward one another, and only near the end of this interval does sudden acceleration occur to produce cluster coalescence.

As virtual time s increases, the steepest descent process in the full 400-particle system first causes particle pairs to form, which then to grow into larger clusters as they combine with monomers and previously formed dimers, trimers, etc. These aggregation processes amount to a local scavenging phenomenon, creating larger and larger empty zones around already-formed clusters. The time-scale expansion indicated in Eq. (4.4) above for dimerization can be adapted to larger clusters, with qualitatively the same result. Growth of distances between neighboring clusters implies greater and greater chronological separation between distinct cluster in-fall and aggregation events. Consequently, numerical integration of the steepest descent equations evolves into an intermediate stage consisting of long intervals during which little cluster movement and little change in Φ occurs, separated by sudden events in which pairs of clusters combine and Φ drops quickly to a lower value. In the later stages of the numerical integration, on account of this time dilation effect, sequences of lengthy runs were executed, each comprising 3×10^6 steps.

Owing to the extreme slowness of the later stages of steepest descent for dilute systems such as that under study here, it has proved impractical to utilize that procedure alone to identify the final inherent structure. Instead, while following the steepest descent operation as it produces a collection of relatively large isolated clusters, the numerical procedure switched repeatedly to a much more efficient variant, the quasi-Newton MINOP method for locating minima (Kaufman, 1999). It needs to be stressed that the MINOP procedure does not interrupt the steepest descent process, but only utilizes its instantaneous particle configurations as its own input. An alternative procedure that might have served about as well as MINOP is the standard conjugate gradient method (Press et al., 1986). Neither of these alternative procedures strictly follow the multi-dimensional gradient direction, but in the low density regime both have the capacity to hop over low ridges on the Φ hypersurface that for dilute systems apparently are present in great profusion. This is actually a substantial advantage for the present investigation, because it creates access to a wide collection of inherent structures. In principle, the collection of MINOP outputs is essentially equivalent to strict application of the steepest descent mapping, but from a distribution of distinct starting configurations. Results presented in Section 5 show system configurations both before and after implementation of this minimizing scheme.

5. Results

As empty scavenged zones develop around particle clusters, counting those clusters and classifying them by numbers of included particles becomes essentially unambiguous. The only uncertainties occur during those short time intervals during which cluster aggregation processes are underway. In any case, discrete clusters can be identified by a precise "physical cluster" criterion that is based on a pair-distance connectivity criterion to decide inclusion or exclusion (Stillinger, 1963). Suppose this has been done, and then let $n_k(s)$ denote the number of clusters containing exactly k particles, present at virtual time s. Then for the present series of calculations these numbers satisfy the condition:

$$400 = \sum_{k=1}^{400} kn_k(s) \quad (5.1)$$

and yield the average cluster size at virtual time s:

$$\langle k \rangle = 400 \bigg/ \sum_{k=1}^{400} n_k(s). \quad (5.2)$$

Fig. 3 presents a system configuration that started as shown in Fig. 2, after the aggregation process driven by the steepest descent process has been underway, but still in a relatively early stage. The virtual time that has elapsed at this snapshot is $s \cong 4770$. This configuration presents 74
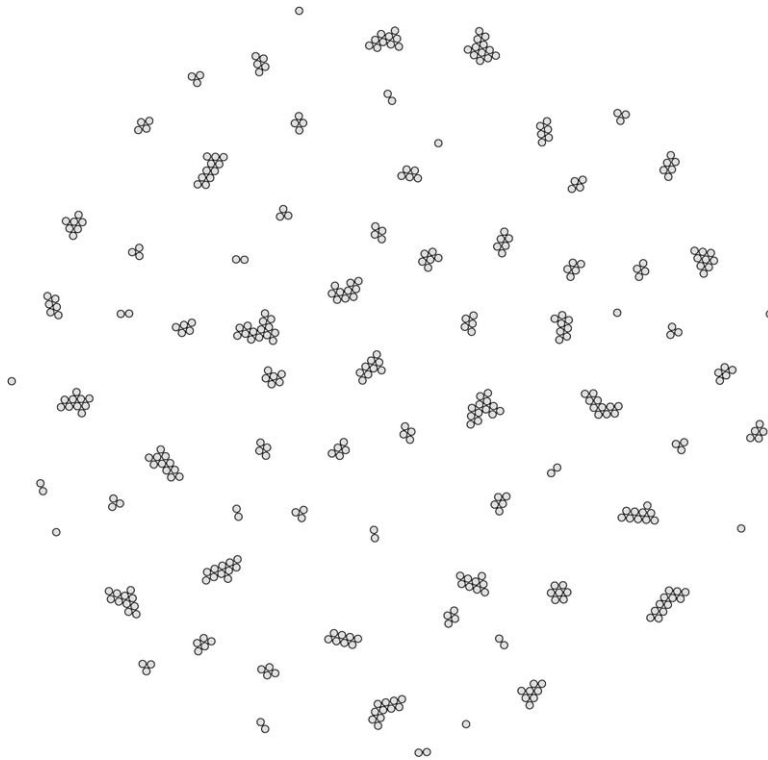
Fig. 3. Early-stage configuration showing cluster aggregation. The virtual time that has elapsed during the steepest descent process is approximately 4770. At this stage the average cluster size is 5.41 particles.

distinguishable clusters, for a mean cluster size $\langle k \rangle \cong 5.41$. The potential energy at this stage of the steepest descent process is $\Phi \cong -614.533$.

The system configuration at a substantially later stage of the steepest descent operation appears in Fig. 4. The elapsed virtual time at this snapshot is $s \cong 423,000$. The potential energy has declined to $\Phi \cong -803.261$. Aggregation has reduced the number of distinct clusters to 19 (average cluster size $\langle k \rangle \cong 21.05$). The mean gap between neighboring clusters has widened considerably, in comparison with that of the preceding Fig. 3 (the plotting length scales are virtually the same for the two figures). It also should not escape attention that most of the clusters present rather non-compact shapes, evidently reflecting the preferred directions along which the steepest descent process has brought the component smaller fragments into contact. More specifically, clusters tend to be attracted to, and to attach to, one another at their most protuberant portions as a result of the rather short range of the LJ forces.

Figs. 5–9 provide a sampling of the inherent structures for the 400 LJ particles, generated from

intermediate-stage configurations of the steepest descent process. The order of their appearance in these figures corresponds to increasing virtual time of the steepest descent process that supplied the initial configurations for MINOP. In the authors' opinion, these figures convey at least qualitatively the types of tenuous final aggregation patterns that can occur when just a single connected cluster appears. These five examples have been selected from the collection of 92 inherent structures generated for the 400 LJ particles, no two of which were identical in structure or energy.

The captions to Figs. 5–9 state the respective values of potential energy Φ for those inherent structures shown. These values lie well within the upper and lower bounds for all inherent structures for 400 LJ particles in the unbounded plane. As mentioned above, the upper bound corresponds to the fully extended needle configuration. Our calculations suggest that the lower bound, the lowest-lying inherent structure, involves an hexagonal piece of the triangular lattice, comprising 397 particles (a "perfect hexagon number" of the form $3n^2 - 3n + 1$), augmented by the remaining three particles
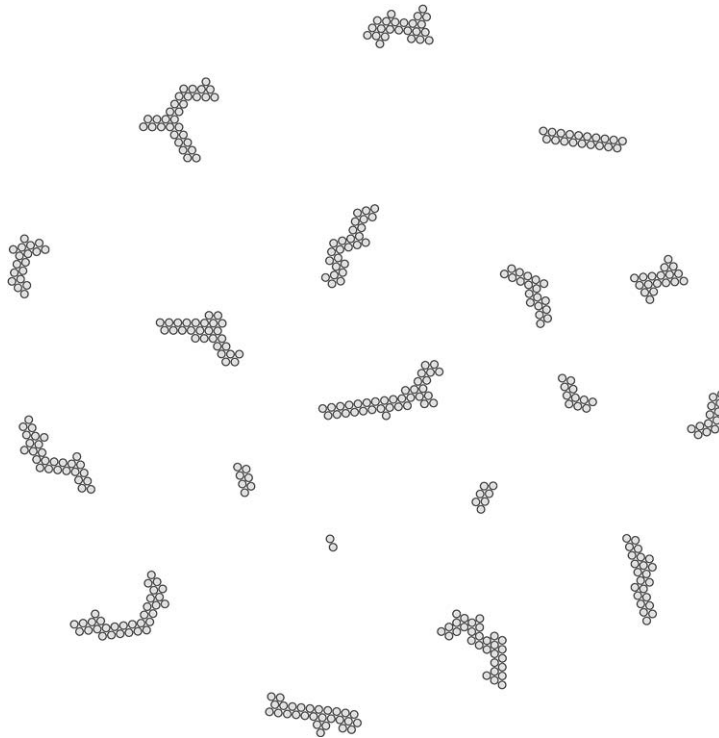
Fig. 4. Intermediate stage configuration during the steepest descent process, following that shown in Fig. 3. The elapsed virtual time at this point is approximately 423,000, and the average cluster size is 21.05.
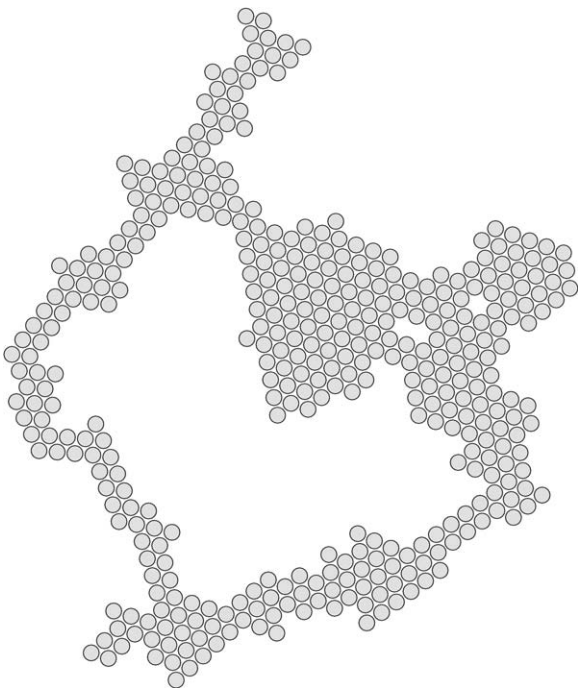

Fig. 5. Inherent structure generated from the intermediate-stage configuration of the steepest descent operation, shown above in Fig. 3. The potential energy is −1041.704.
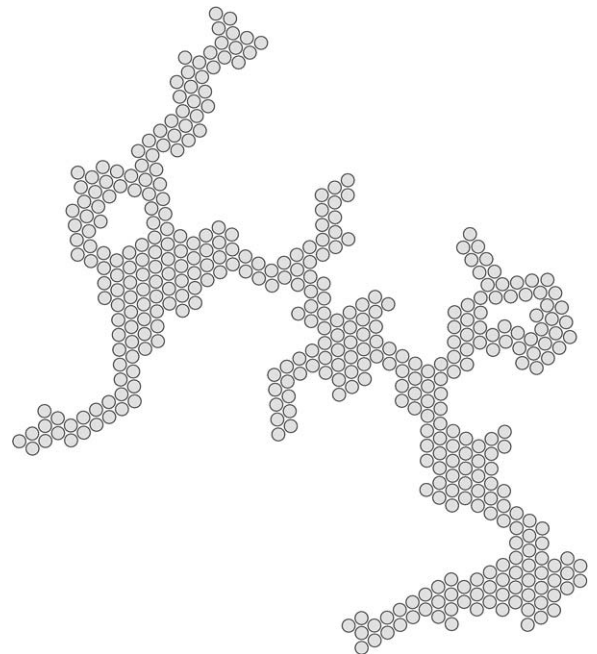

Fig. 6. Inherent structure generated from an intermediate stage of the steepest descent procedure. The potential energy of this configuration is −976.705.
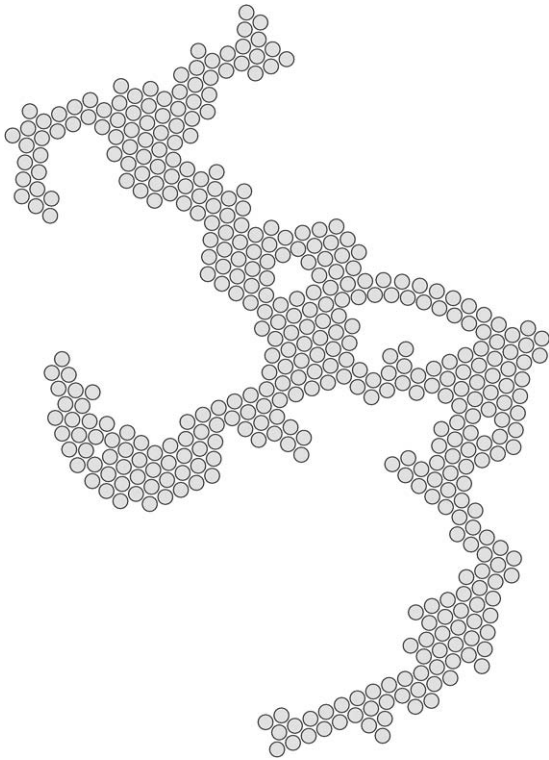
Fig. 7. Inherent structure generated from an intermediate stage of the steepest descent procedure. The potential energy of this configuration is −1009.080.

Fig. 8. Inherent structure generated from an intermediate stage of the steepest descent procedure. The potential energy of this configuration is −967.687.

resting together midway on one side of the hexagon. Consequently, all 400-particle inherent struc-
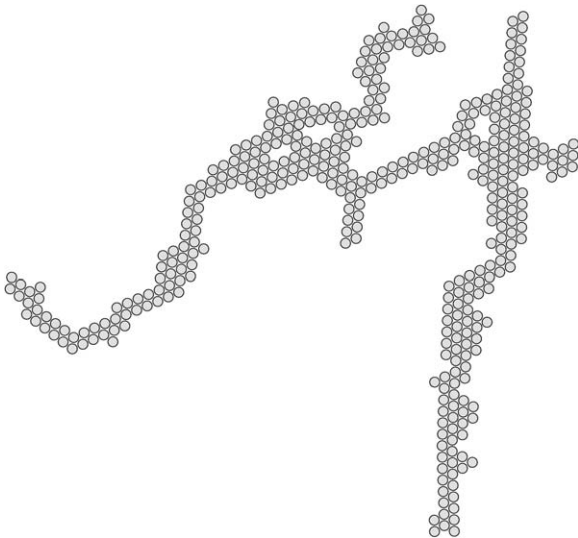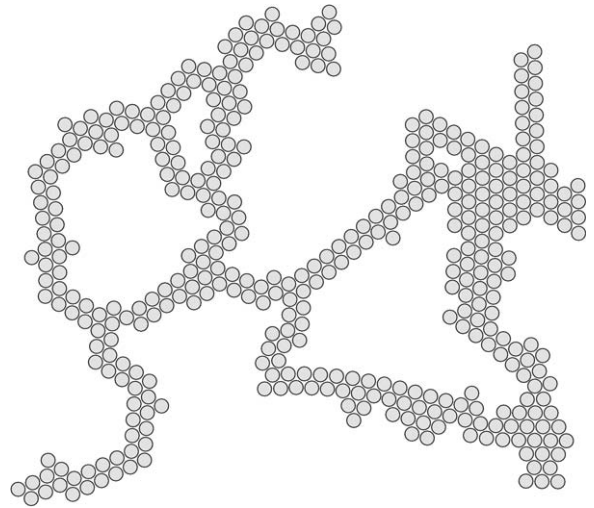

Fig. 9. Inherent structure generated from an intermediate stage of the steepest descent procedure. The potential energy of this configuration is −936.838.

ture energies apparently must lie within the interval:

$$-843.097 \geqslant \Phi \geqslant -1263.247. \qquad (5.3)$$

The average value of the 92 inherent structure energies constructed from the steepest descent trajectory is:

$$\langle \Phi \rangle = -1001.189. \qquad (5.4)$$

The fact that this average is significantly closer to the upper limit in Eq. (5.3) than to the lower limit evidently illustrates the statistical preponderance of non-compact particle arrangements, with correspondingly reduced numbers of close particle contacts. The highest and lowest values obtained for inherent structures during the simulation were −929.707 and −1091.372, respectively. Furthermore, examination of the entire set of 92 inherent structures shows the expected steady trend toward more compactness as energy descends over this interval. It is reasonable to suppose that if the steepest descent process had started with the 400 particles randomly dispersed over a larger circular area, the resulting inherent structures would have tended to be even more tenuous and higher in average potential energy.

The inherent structure presented in Fig. 5 was generated from the steepest-descent-mapping configuration that appeared earlier in Fig. 3. This provides a clear example of the occurrence of large portions of empty space that are often found

enclosed by particle bridges formed from subsets of the full 400 particle system. They are a key structural element in the formation of two-dimensional expanded matter with the LJ interaction. The case shown in Fig. 6 illustrates multiple branching, to produce a dramatically non-convex outer contour of the inherent structure. Neighboring branches around such a contour can be regarded as incomplete enclosures of empty space, and if a substantially larger number of LJ particles than 400 had been considered in the calculation, enclosure could well have occurred. Fig. 7 displays a medium-sized cavity that is partly surrounded by a strongly curved bridge amounting to a stressed portion of a needle structure. Fig. 8 demonstrates how thin a profile can arise in what is nominally a mechanically stable (but no doubt rather fragile) arrangement of the 400 LJ particles. The final example, Fig. 9, can credibly be argued as representing the beginning of the growth of a larger spongy structure, pervaded with large voids.

Some of the voids appearing in the inherent structures can simply be identified as cases of missing-particle clusters within what would otherwise be locally a close-packed (triangular) crystal arrangement. The simplest of these are the monovacancy (bounded by six neighboring particles) and the divacancy (eight neighboring particles), single examples of which both appear in Fig. 5. Depending of course on the number of LJ particles available to form an inherent structure, polyvacancies of arbitrarily large size are possible. However, many other cavity types also arise, which cannot simply be identified as polyvacancies, but are associated with crystal dislocations. The two voids in Fig. 8, that are larger than its divacancy, have this character. For both of these, hypothetical attempts to fill them with extra particles would yield a small void surrounded by five neighboring particles, not six as with a monovacancy. Other examples exhibit seven neighboring particles either directly, or after hypothetical particle additions.

Generally, the voids can be classified according to their "Burgers vector" (Meyers, 1997). Voids that are simple monovacancies, divacancies, or polyvacancies have vanishing Burgers vectors. The remaining cases have non-vanishing Burgers vectors specifying the amount of local strain that has to be imposed on an unstrained lattice in order to match up the contacting lines of particles that remain around the cavity. These strain-exhibiting particle arrangements amount to dislocations in the underlying triangular lattice structure. Fig. 7 exhibits a case of substantial strain manifested as strong inward curvature. When a non-vanishing Burgers vector is present (always a multiple of the lattice vector), the lines of particles surrounding the void curve inward or outward, depending on the local direction of that vector. Inherent structures for large numbers of LJ particles in an expanded solid state can simultaneously exhibit voids with a variety of Burgers vectors.

6. Discussion

The existence of many diverse expanded (low density) forms of matter depends on the capacity of those materials' constituent particles to adopt mechanically stable arrangements (inherent structures) that incorporate substantial void space. This capacity evidently can arise from a wide variety of binding interactions, and it remains a challenge to determine how details of those interactions quantitatively influence the specific properties of the expanded solids at both the molecular and macroscopic levels. The present investigation offers a small contribution to this subject. It has been restricted to particle aggregation in two dimensions, and has utilized the very simple and theoretically popular Lennard-Jones (LJ) pair potential. In spite of these simplifications, the results obtained from the cooperative aggregation process considered exhibit several non-trivial and informative properties.

The scenario considered starts with a dilute gaslike arrangement of 400 point particles, confined for convenience only at the outset to the interior of a large circle. Forces between these particles are specified uniquely by the LJ pair interactions present. The initial particle configuration is subsequently deformed by the steepest-descent process (Eq. (3.1)), moving the particles toward a mechanically stable potential energy minimum (an "inherent structure"). For practical reasons, the later stages of the minimization process are handled by an efficient function minimization routine (MINOP). As a result of repeated application of that latter routine at regularly spaced times of the steepest descent it has been possible to generate a large collection of inherent structures characteristic of a dilute vapor.

The representative samples of the inherent structures produced in this investigation, shown in Figs. 5–9, illustrate the ability of the LJ model of interacting particles to aggregate into a wide variety of spatially extended structures. These low-density solid

structures can be highly branched, and can enclose void space that ranges in size from single missing particles (monovacancies) to holes of much larger size limited only by the fixed number of particles present in the calculations. Furthermore, these spatially extended inherent structures can, and usually do, incorporate elements of disorder and strain associated with non-vanishing Burgers vectors. The average value of the binding energy for this collection of inherent structures has been found to lie significantly closer to the upper limit for 400 LJ particles than to the lower limit, owing to the large fraction of the 400 that reside at the external and internal surfaces of the extended, branched, void-containing inherent structures. Such geometric patterns of course cannot arise from a system constrained to high density. These observations confirm the assumptions that were previously invoked to analyze the enumeration of distinguishable inherent structures in the low-density regime (Stillinger, 2001).

Of course it is highly desirable to extend the present simple two-dimensional modeling to three dimensions. Even retaining the LJ interaction in that extension, some important changes can be anticipated. First, the void space within the interior of a spatially extended inherent structure can be connected to the exterior by means of tunnels, either simple or multiply branched. Second, the locally dense regions packed with LJ particles in three dimensions have many possible amorphous arrangements, in contrast to the obvious local crystalline order that is evident in the two-dimensional examples exhibited in Figs. 5–9. Third, though likely to be rare, is the possibility in three dimensions that separate bridges of particles, both attached to the main body of an inherent structure, can geometrically pass through one another without touching. In any case, one expects the preponderance of inherent structures formed in unbounded three-dimensional space to have the same strong statistical tendency toward spatial extension, and to reinforce the same qualitative assumptions about enumeration that apply to the two-dimensional scenario.

It is perhaps inevitable that the present inherent structure generation method, based on the steepest-descent mapping operation, should be compared and contrasted with the so-called "diffusion-limited aggregation" (DLA) process (Witten and Sander, 1981; Meakin, 1983). Both techniques produce ensembles of spatially extended cluster structures

for which the concept of "fractal dimension" may become applicable in the large-system limit. However, DLA is a sequential process, by which single particles are added irreversibly to a growing cluster. The present approach is concurrent, i.e. all particles present in the final inherent structure are present from the outset, initially causing formation of small clusters that eventually combine to produce the final single aggregate. The DLA results tend to be highly dendritic, that is, consisting of radially diverging thin branches that in two dimensions seldom enclose void space disconnected from the exterior space. Most DLA simulations use an underlying discrete lattice of available particle positions, and so cannot produce structures for which non-vanishing Burgers vectors are present. DLA processes do not involve a potential energy function, one of the basic elements of the present modeling.

One of the obvious limitations of the present approach is that it cannot directly address the very low density regime of particle aggregation. Although attractive LJ forces are present at any large distance between pairs of particles, it becomes impractical to attempt any numerical study of steepest-descent mapping when the average distance between neighboring particles in the initial configuration is very large. Nevertheless, it is reasonable to extrapolate from the present observations into the very dilute regime with the conclusion that for sufficiently large particle number N, the typical inherent structures that would be produced would be even more extended. If one were to imagine surrounding each final configuration with a convex envelope, the density of points within that envelope would approach zero in the large-N, zero-initial-density limit.

Although the calculations reported in this paper have utilized a circle-herded initial configuration embedded in an infinite space, alternative boundary condition choices should eventually be examined. An obvious alternative is periodic boundary conditions, for example with a square (two dimensions) or cubic (three dimensions) primary cell containing N particles, surrounded on all sides by a periodic array of image cells extending to infinity. Upon reduction to corresponding mechanically stable inherent structures, this would provide an approximation to an infinitely extended expanded solid with density determined by the choice of primary cell size. Considering the clear tendency toward aggregate non-compactness exhibited by the results of the present study, it seems clear that results likely to emerge with periodic boundary conditions will

be above the percolation threshold (i.e. globally connected throughout all space) unless the density was very low. It will be instructive in the long run to determine, for any given interaction, what density represents that percolation threshold.

Returning finally to the silica aerogel example mentioned at the outset, we remind the reader that reasonably accurate potential energy functions have been published for SiO_2 and that these are available for study of low-density inherent structures using the kinds of strategies considered in this paper (Tsuneyuki et al., 1988; van Beest et al., 1990). Among other issues that deserve attention, such simulations could determine the similarities and differences in chemical bonding characteristics between aerogels and solid amorphous silica, and the chemical reactivity of the surface of the aerogel inorganic network to foreign species such as water and hydrogen fluoride.

References

Brydson, J.A., 1989. Plastics Materials, fifth ed. Butterworths, London, pp. 426–430.

Della Valle, R.G., Venuti, E., Brillante, A., Girlando, A., 2003. Inherent structures of crystalline pentacene. J. Chem. Phys. 118, 807–815.

Engh, T.A., 1992. Principles of Metal Refining. Oxford University Press, Oxford, p. 154.

Frick, J., 1988. Aerogel. Sci. Am. 258, 92–97.

Giovambattista, N., Starr, F.W., Sciortino, F., Buldyrev, S.V., Stanley, H.E., 2002. Transitions between inherent structures in water. Phys. Rev. E 65, 041512.

Jones, J.E., 1924. On the determination of molecular fields. II. From the equation of state of a gas. Proc. R. Soc. Lond. Ser. A 106, 463–477.

Kaufman, L., 1999. Reduced storage, quasi-Newton trust region approaches to function optimization. SIAM J. Optim. 10, 56–69.

Kiryukhin, V., Keimer, B., Boltnev, R.E., Khmelenko, V.V., Gordon, E.B., 1997. Inert gas solids with nanoscale porosity. Phys. Rev. Lett. 79, 1774–1777.

Kong, I., Soh, H.T., Cassell, H.M., Quate, C.F., Dai, H.J., 1998. Synthesis of individual single-walled carbon nanotubes on patterned silicon wafers. Nature 395, 878–881.

Krätschmer, W., Lamb, L.D., Fostiropoulos, K., Huffman, D.R., 1990. Solid C_{60}: a new form of carbon. Nature 347, 354–358.

Meakin, P., 1983. Diffusion-controlled cluster formation in two, three, and four dimensions. Phys. Rev. A 27, 604–607.

Meyers, H.P., 1997. Introductory Solid State Physics, second ed. Taylor & Francis, London, pp. 81–86.

Pekala, R.W., Hrubesh, L.W. (Eds.), 1995. Proceedings of the Fourth International Symposium on Aerogel. North Holland, Amsterdam, J. Non-Cryst. Solids 186 (1995).

Press, W.H., Flannery, B.P., Teukolsky, S.A., Vetterling, W.T., 1986. Numerical Recipes. Cambridge University Press, Cambridge (Section 10.6).

Sheely, W.F., 1967. Radiation EffectsMetallurgical Conferences, vol. 37. Gordon and Breach, New York.

Sheng, H.W., Ma, E., 2004. Atomic packing of the inherent structure of simple liquids. Phys. Rev. E 69, 062202.

Stillinger, F.H., 1963. Rigorous basis of the Frenkel–Band theory of association equilibrium. J. Chem. Phys. 38, 1486–1494.

Stillinger, F.H., 2001. Inherent structures enumeration for low-density materials. Phys. Rev. E 63, 011110.

Stillinger, F.H., Stillinger, D.K., 1990. Computational study of transition dynamics in 55-atom clusters. J. Chem. Phys. 93, 6013–6024.

Stillinger, F.H., Weber, T.A., 1983. Dynamics of structural transitions in liquids. Phys. Rev. A 28, 2408–2416.

Tsuneyuki, S., Tsukuda, M., Aoki, H., Matsui, Y., 1988. First-principles interatomic potential of silica applied to molecular dynamics. Phys. Rev. Lett. 61, 869–872.

van Beest, B.W.H., Kramer, G.J., van Santen, R.A., 1990. Force fields for silica and aluminophosphates based on ab initio calculations. Phys. Rev. Lett. 64, 1955–1958.

Witten, T.A., Sander, L.M., 1981. Diffusion-limited aggregation, a kinetic critical phenomenon. Phys. Rev. Lett. 47, 1400–1403.